Correlation of β–value with Spreading Rate for Strike-slip Earthquakes of the Mid-Oceanic Ridge System

Amy R. Langenhorst[1] and Emile A. Okal

Department of Geological Sciences, Northwestern University, Evanston, Illinois

We present a regionalized study of the frequency-moment characteristics of strike-slip earthquakes occurring on transform faults of 12 segments of the Mid-Oceanic Ridge system. We observe a remarkable correlation between the β–value obtained at the lower-moment end of the population, and the regional spreading rate V. Similarly, the elbow moment expressing the saturation of fault width decreases with increasing V. By combining a scale invariant model for the population of earthquakes on a given transform fault with a similar power law for the population of offset lengths along a given ridge, we build a model explaining most of our observations, and in particular the growth of β with spreading rate. The only exceptions to our model are the Southeastern and Southwestern Indian Ocean Ridge systems, where local conditions probably affect the distribution of transform offsets.

1. INTRODUCTION

Although oceanic transform faults [TF] host largely passive plate boundary processes involving neither creation nor consumption of lithosphere, they contribute significantly to global seismicity, as documented by the size of the largest TF earthquake ever recorded, the 1942 event on the Andrew Bain Fracture Zone ($M_s = 8.1$; $M_0 = 1.35 \times 10^{28}$ dyn-cm) [*Okal and Stein*, 1987]. Since spreading rates at Mid-Oceanic Ridges [MOR] vary by more than one order of magnitude, the thermal evolution of young oceanic plates features lateral heterogeneity. The 60,000–km long MOR system, and especially its TF segments, is thus a natural laboratory for the study of various plate tectonics processes under relatively simple physical conditions: to a large extent, the evolution of geological structures is controlled by the variation of a single parameter, namely the spreading rate, and left unmarred by the many unrelated processes involved in continental areas.

In this general framework, the purpose of the present paper is to analyze the frequency-moment population statistics for strike-slip earthquakes occurring on oceanic TFs, and to propose a possible model explaining the reported difficulty to fit even regional datasets of such events with a simple power law expressing a Gutenberg-Richter relationship. Our approach is based on combining scale-invariant population models both for the occurrence of various sizes of earthquakes on a given TF and the occurrence of TFs of various offset lengths along a given MOR segment.

Frequency-magnitude relationships were first proposed by *Gutenberg and Richter* [1942], before the concept of scalar seismic moment, M_0, allowed a physically rigorous

[1]Presently at: Geophysical Fluid Dynamics Laboratory, Princeton, New Jersey.

Plate Boundary Zones
Geodynamics Series 30

10/1029/030GD11

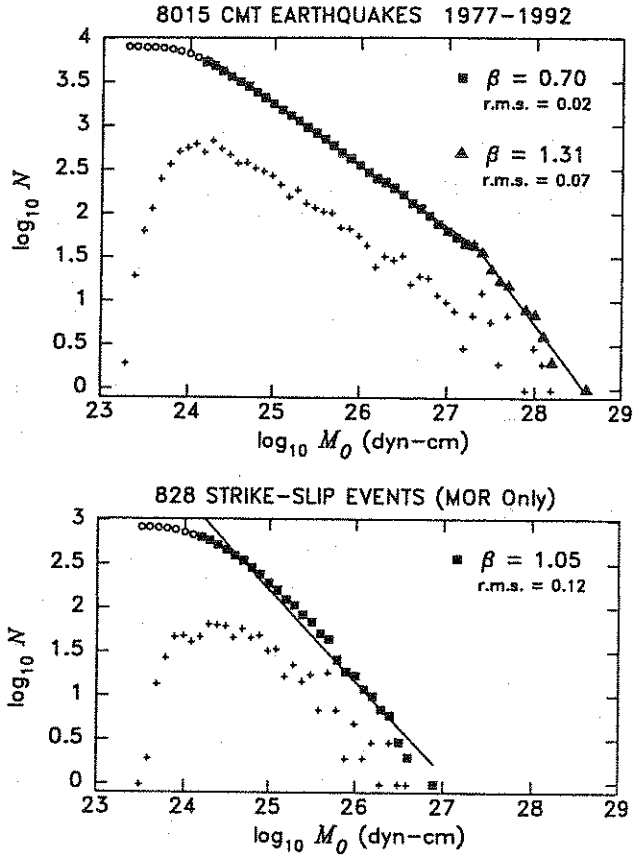

Figure 1. *Top:* Frequency-moment relationship for the full dataset of CMT solutions studied by *Okal and Romanowicz* [1994]. *Bottom:* Frequency-moment relationship for the dataset of MOR strike-slip earthquakes used in that study. Note the curvature of the latter distribution, poorly fit by a a two-segment model; the steeper slope of the best-fitting single-line model; and the poorer quality of the fit, as expressed by the root-mean-square residual. On both diagrams, earthquakes are binned into windows of width 0.1 logarithmic unit. The + signs represent the incremental number of earthquakes in each bin; the larger symbols the cumulative numbers (with moments greater than M_0); the solid symbols represent the segments along which a best-fitting regression, shown by a straight line, is carried out; the open ones illustrate the lack of completeness of the dataset due to undersampling of the catalogue at lower moments. Results from the regression (β–value and root-mean-squares residual) are shown at right. Adapted from *Okal and Romanowicz* [1994].

quantification of earthquake sources. As detailed by *Okal and Romanowicz* [1994], the use of magnitude scales rather than moments brings the additional difficulty of the saturation of the magnitude scale, which can combine with, and thus obscure, some intrinsic physical properties inherent in the earthquake population. For this reason, in the present study, we quantify earthquake populations using exclusively the β–value introduced by *Molnar* [1979], writing the number of earthquakes $N(M_0)$ with a moment at least equal to M_0 as:

$$\log_{10} N = \alpha - \beta \log_{10} M_0 \qquad (1)$$

where the parameter α depends on the particular subset of events selected, *e.g.*, the duration of the time window sampled.

Rundle [1989] has shown that, under the assumption of scale invariance, β is predicted to take the value 2/3. In lay terms, this assumption is equivalent to saying that an element of fault has the same probability of seeing its strain released through an earthquake of any size. Further work by *Romanowicz and Rundle* [1993] has shown that, as the size of the earthquake grows, the transverse (mostly vertical) dimension of the faulting area saturates due to penetration of the brittle-ductile transition, leading to the development of an elbow in the frequency-size curve, with greater values of β (in principle, β = 1) at larger moments. As discussed by *Okal and Romanowicz* [1994], this model readily explains the frequency-moment statistics of the global CMT catalogue of shallow earthquakes ($h \leq 75$ km), as well as many subsets of events, such as interplate thrust earthquakes, normal faulting events, or even shocks along large continental strike-slip faults.

However, strike-slip earthquakes along transform faults of the MOR system cannot be easily modeled by a two-segment regression curve: no clear elbow can be defined, and a single-segment regression gives both a higher β–value (1.05) and a poorer fit than for the full CMT dataset, as summarized on Figure 1. *Okal and Romanowicz* [1994] explained this observation qualitatively by noting that the saturating depth D in their model is locally controlled by the temperature field along the walls of the fault, itself a function of length of offset, l, and spreading rate, V. Thus, D is expected to be highly variable among TFs, and the global population of MOR events might not be well fit by *Romanowicz and Rundle*'s [1993] two-segment model. In the present paper, we examine this possibility systematically by breaking down the population of strike-slip TF earthquakes into regional subsets for which spreading rate can be considered constant, and studying the resulting population statistics in each region. We observe a correlation, holding for most spreading centers, between V and the β–value best-fitting the low-moment end of the earthquake population.

Few other studies of earthquake population statistics specifically targeted oceanic TFs: *Frohlich and Davis* [1993] sorted events by focal mechanism, but did not separate oceanic strike-slip sources from continental ones; in contrast *Kagan* [1997] studied MOR seismicity, but regrouped earthquakes on ridge segments and TFs; later, *Kagan* [1999] focused mostly on continental areas. More recently, and concurrently to the present study, *Bird et al.* [this volume] examined frequency-moment characteristics both on spreading segments and TFs. We briefly compare our results with theirs in Section 4. Note that we do not seek to model TF populations with the more elaborate statistics such as the γ distribution [*Kagan,* 1993]. We will see that *Romanowicz and Rundle*'s [1993] model, based on a set of very simple and universal physical assumptions, can explain most of our observations.

2. DATASET AND METHODOLOGY

We consider here all 1037 strike-slip earthquakes reported on the MOR system in the Harvard CMT catalogue [*Dziewonski et al.,* 1983 and subsequent quarterly updates], for the time window 1977–1998. We define as strike-slip those events whose null (N) axis dips steeper than 60°, and thus eliminate normal faulting solutions occurring on spreading segments, as well as any earthquakes featuring anomalous focal mechanisms along the TF offsets, as described for example by *Engeln* [1985]. We then split the dataset into 12 regional subsets corresponding to individual plate boundaries, along each of which the spreading rate can be regarded as constant. In each of these regions, we regress the dataset using the algorithm of *Okal and Romanowicz* [1994]. It consists of binning the population into moment windows (we use a constant width, $d\log_{10}M_0 = 0.1$ logarithmic units). The incremental population (plotted as + signs on Figures 2*a–l*) is used to estimate the threshold moment above which completeness is expected. The cumulative population is shown as larger symbols (open ones below the threshold of completeness), and is regressed by fitting a straight line in a selected interval of moments; the opposite of its slope is the β value. When a change of regime is evident on the cumulative plot, a regression is carried out separately in both windows, and the elbow moment identified. When no elbow can be defined, the regression is carried out on the entire dataset, above the completeness threshold.

3. RESULTS

The various frames in Figure 2 present the results of our regressions in the 12 regions. The top part of each frame gives a map of the events used, and the bottom part illustrates the population statistics. For each of the regressions, we focus on the lower range of moments, where saturation should have no effect on source scaling. Estimates of error bars on β are obtained under the simplifying assumption of unknown errors on the individual measurements of the number of events in each bin [*Press et al.,* 1986, p. 507].

It is immediately apparent that the resulting β–values vary widely, from a maximum of 1.47 along the East Pacific Rise (EPR) to a minimum of 0.47–0.48 along the Southwest Indian Ocean Ridge (SWIOR), the Central and Southwest Atlantic. We eliminate the latter two regions from further discussion because of the small size of their population samples (less than 30 earthquakes each). In addition, we note that the quality of fit, quantified by the root-means-square residual of the best-fitting straight line in the relevant range of moments, varies significantly across the datasets, as does the critical moment M_c defining the elbow in the distribution.

In very simple terms, our results can be regrouped into three families: a group of five regions (North Atlantic, South Atlantic, Gulf of Aden, Central Indian [CIOR] and Southeast Indian Ocean Rise [SEIOR]) featuring β–values ranging from 0.62 to 0.73, essentially fitting the expected value $\beta = 2/3$; a group of four regions (Chile Rise, Balleny-Tasman, Pacific-Antarctic Rise [PAR] and East Pacific Rise [EPR]) with significantly larger values of β (from 0.91 to 1.47); and the SWIOR, which features a very low value ($\beta = 0.47$). Figure 3 illustrates the remarkable correlation between full spreading rate V and β–value. Values of V were computed in each region by averaging the individual values predicted at each epicenter from the NUVEL-1 model of *DeMets et al.* [1990]. Error bars on V were obtained by averaging the error bars assigned by *DeMets et al.* [1990] to the rate data along the relevant plate boundary.

Figure 4 regroups our results concerning elbow moments M_c. In two regions (PAR and CIOR), no elbow could be resolved. For the other 10 regions, we use scales linear in $M_c^{1/3}$ and $V^{-1/2}$, since we anticipate that both quantities should be linearly related to the maximum thickness of the brittle layer at the center of the TF offset, W_{max} (see Section 4). With the exception of SWIOR, the well-sampled regions do suggest a linear correlation, with a best-fitting slope of 9.4×10^8 [(dyn–cm)$^{1/3}$ * (cm/yr)$^{1/2}$] or 1.7×10^5 c.g.s. units.

4. INTERPRETATION AND DISCUSSION

We illustrate on the case of the Balleny-Tasman region (Figure 2*c*) the departure of the population from the stan-

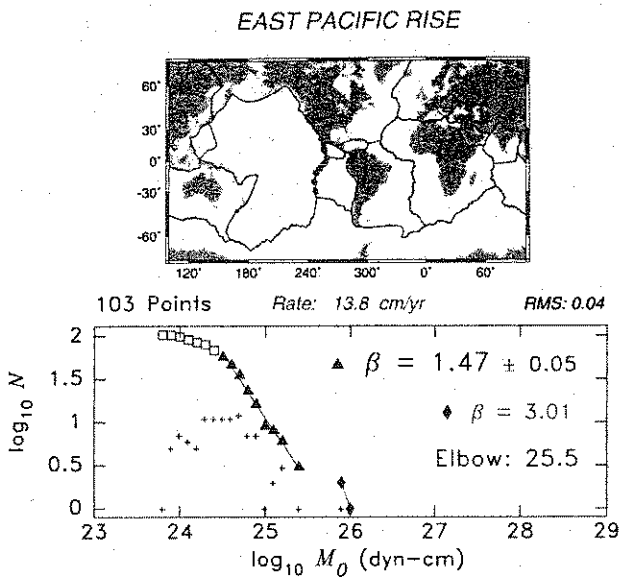

Figure 2*a*. Results for the East Pacific Rise. *Top:* Map showing the location of the individual earthquakes making up the regional dataset. The full rate shown represents an average of NUVEL-1 spreading rates at each epicenter. *Bottom:* Population statistics for the regional dataset. Same conventions as in Figure 1. In addition, the error estimates on β are obtained under the assumption of unknown errors on the individual bin populations [*Press et al.*, 1986].

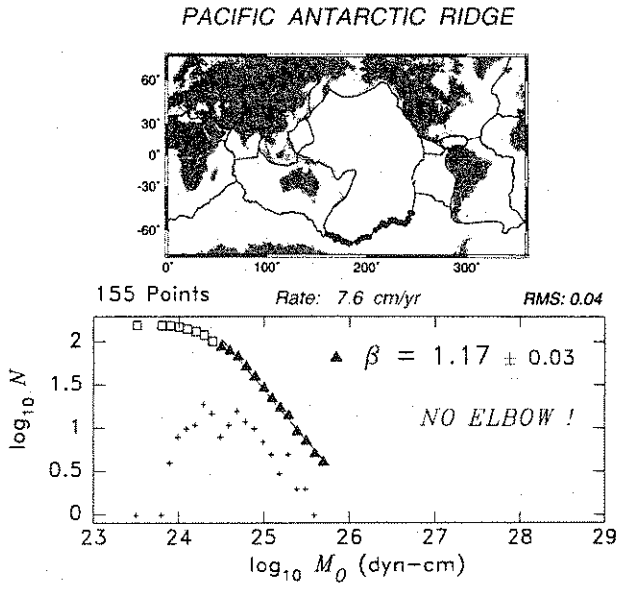

Figure 2*b*. Same as Figure 2*a* for the Pacific–Antarctic Ridge. Note the impossibility to define an elbow in the population, already noted by *Okal and Langenhorst* [2000].

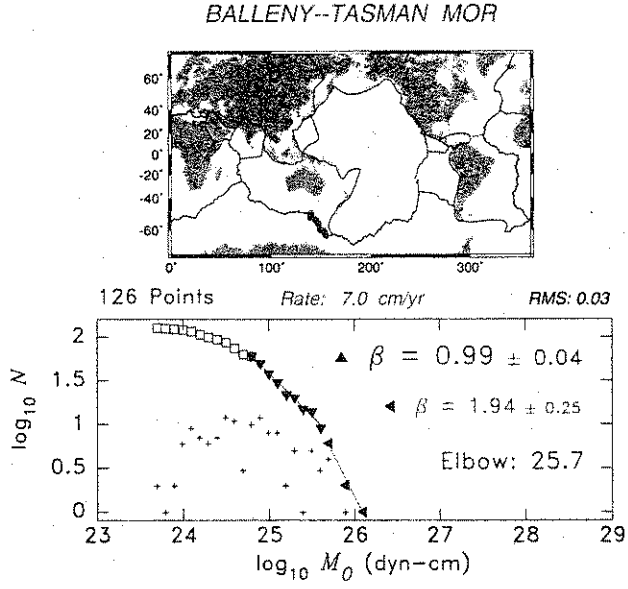

Figure 2*c*. Same as Figure 2*a* for the Balleny–Tasman Region.

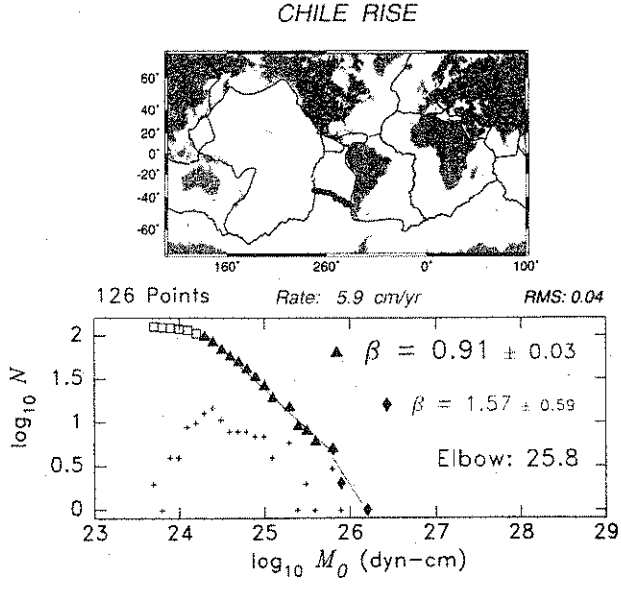

Figure 2*d*. Same as Figure 2*a* for the Nazca–Antarctic boundary along the Chile Rise.

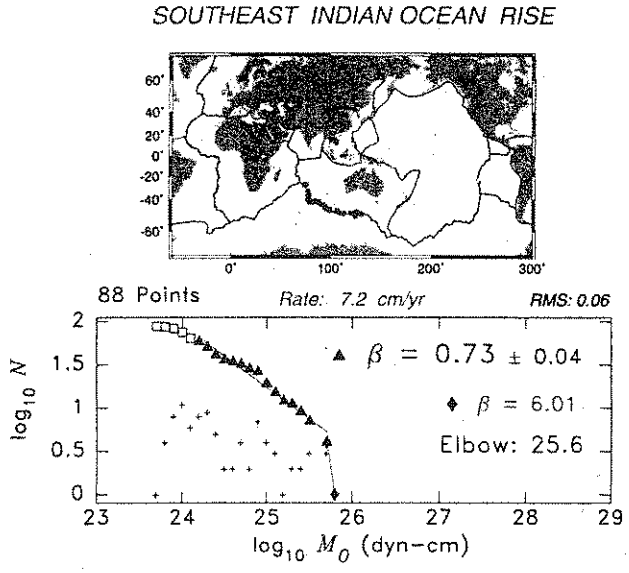

Figure 2*e*. Same as Figure 2*a* for the Southeast Indian Ocean Ridge (SEIOR).

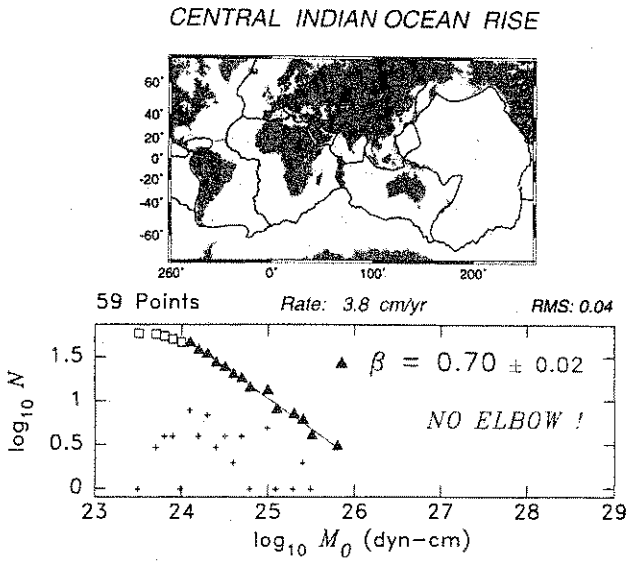

Figure 2*f*. Same as Figure 2*a* for the Central Indian Ocean Ridge (CIOR).

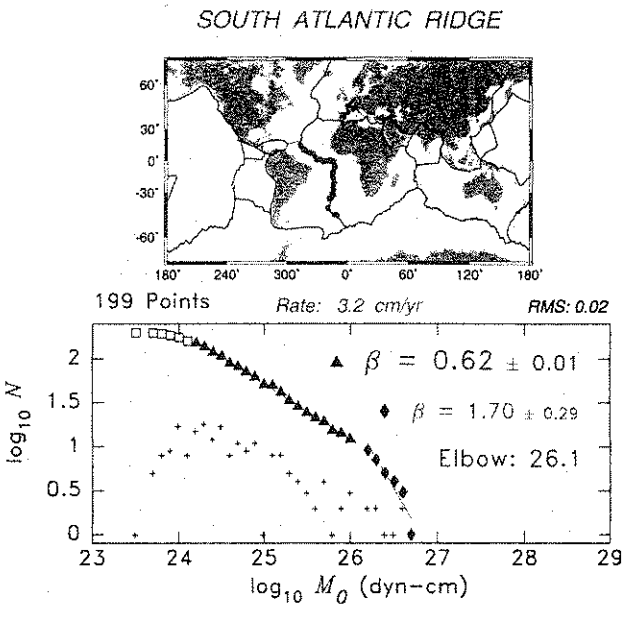

Figure 2*g*. Same as Figure 2*a* for the South Atlantic Ridge.

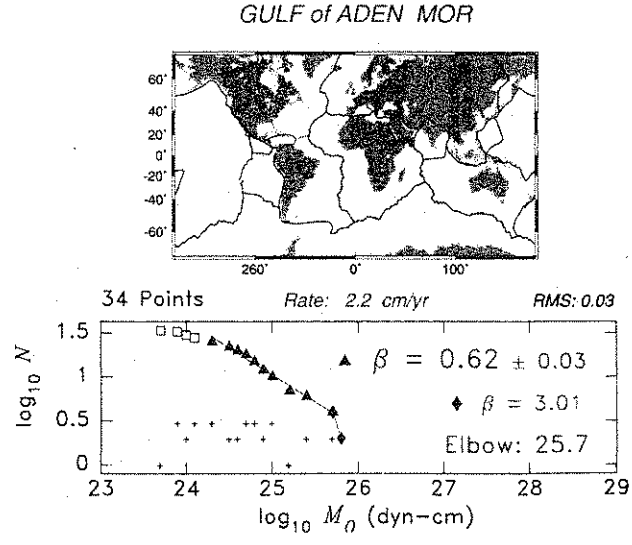

Figure 2*h*. Same as Figure 2*a* for the Gulf of Aden Region.

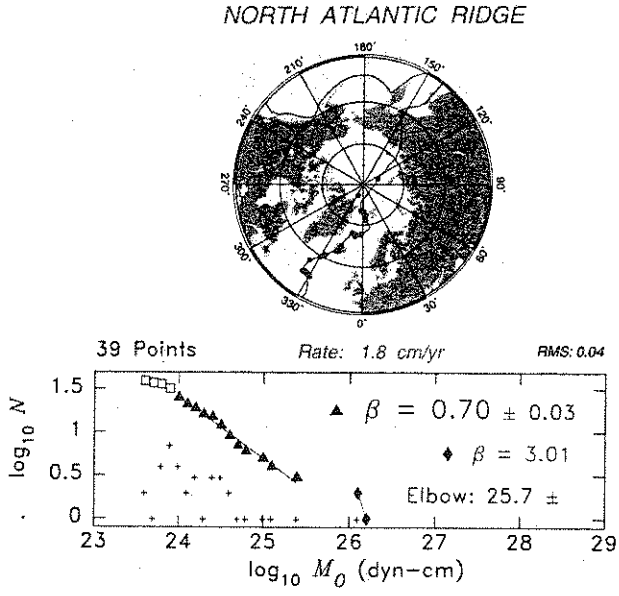

Figure 2*i*. Same as Figure 2*a* for the North Atlantic and Arctic Ridge system.

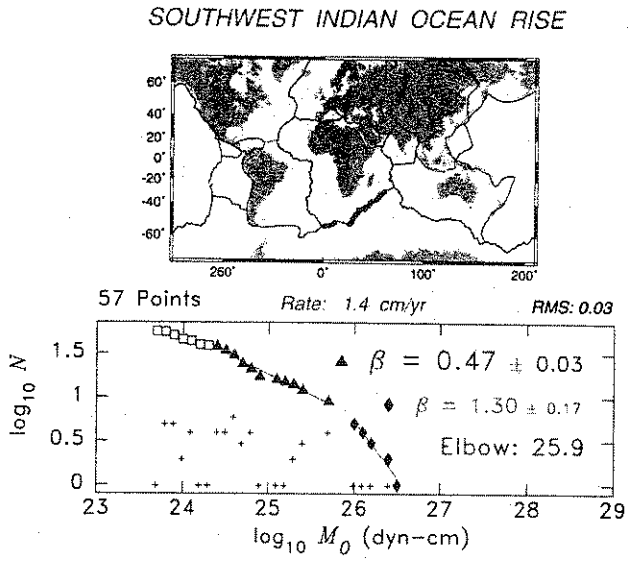

Figure 2*j*. Same as Figure 2*a* for the Southwest Indian Ocean Ridge (SWIOR).

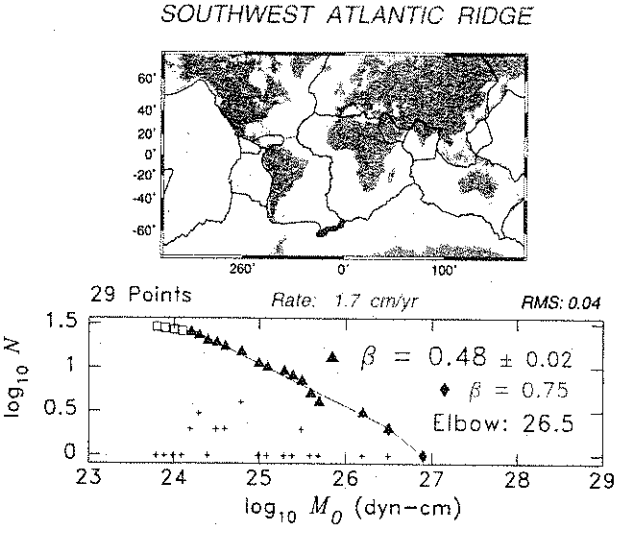

Figure 2*k*. Same as Figure 2*a* for the Southwest Atlantic Ridge. This dataset was not retained because of the small number of earthquakes sampled.

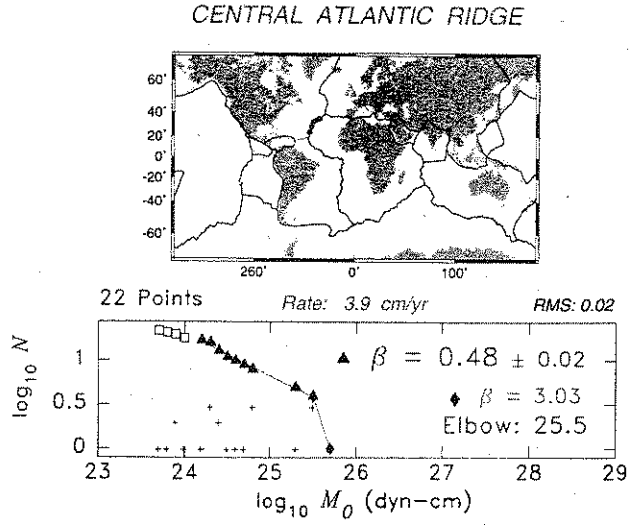

Figure 2*l*. Same as Figure 2*a* for the Central Atlantic Ridge. This dataset was not retained because of the small number of earthquakes sampled.

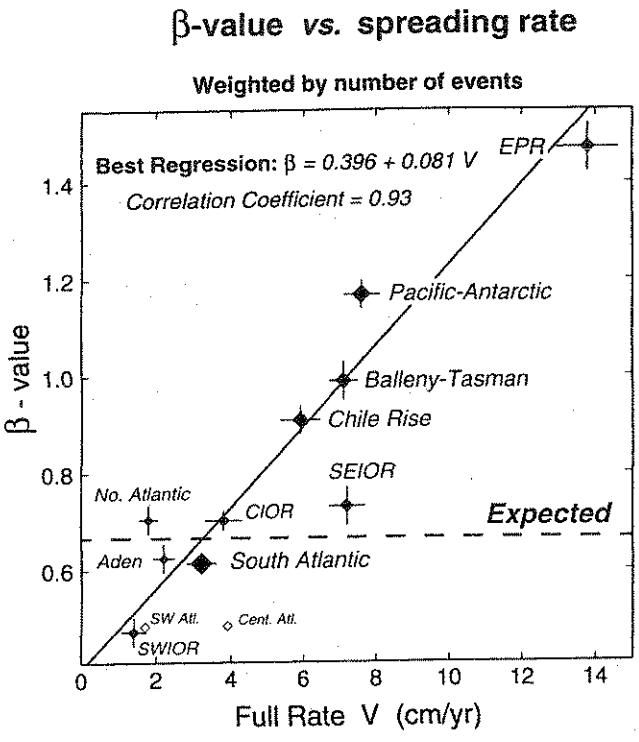

Figure 3. Correlation between spreading rate and β-value. The size of the individual symbols is keyed to the number of earthquakes in each regional dataset. The two regions eliminated from the discussion (Southwest and Central Atlantic) are shown by open symbols. The best regression, weighted by the number of events, is also given. The error bars on β are those determined in Figures *2a-l*, and those on V are estimated from *DeMets et al.* [1990].

dard two-segment model of *Rundle and Romanowicz* [1993]: the distribution shows curvature and is not well fit by straight segments. In addition, the regressed values of β are significantly greater than expected (β = 2/3) from scaling laws. These properties cannot be explained by the simple model of the saturation of fault growth on a single fault plane. Rather, they must express the presence, along a regional MOR system, of TF offsets of variable length l. Each one may feature a two-segment population curve with the slopes β = 2/3 and β = 1 expected theoretically, but each offset has different values of the elbow moment M_c, different maximum-size earthquakes, and different absolute levels of moment release rate, all these parameters being controlled by the length of offset, l. When all such offsets are regrouped into a single dataset, the full population distribution features the curvature evidenced on Figure 2*c*. Finally, note that it would be impossible to study individually the earthquake population statistics of a single TF offset, due to insufficient sampling over the short lifetime of the CMT project.

In order to further explore the influence of spreading rate on population statistics, we need to know the distribution of offset lengths l in a regional context. This problem was examined by *Abbott* [1986], who used three sections of the MOR system to show that TF offsets obey a power law distribution of the form

$$\log_{10} N_l = A - B \log_{10} l \qquad (2)$$

expressing the number N_l of offsets of length greater than l. Her results along the East Pacific, Juan de Fuca and North Atlantic systems suggest that B is essentially equal to 1. This observation sets the stage for building a model of the population of transform fault earthquakes explaining the principal features of the distributions on Figure 2.

We first consider a single TF offset, of length l, part of a segment of MOR opening at a full rate V. Following

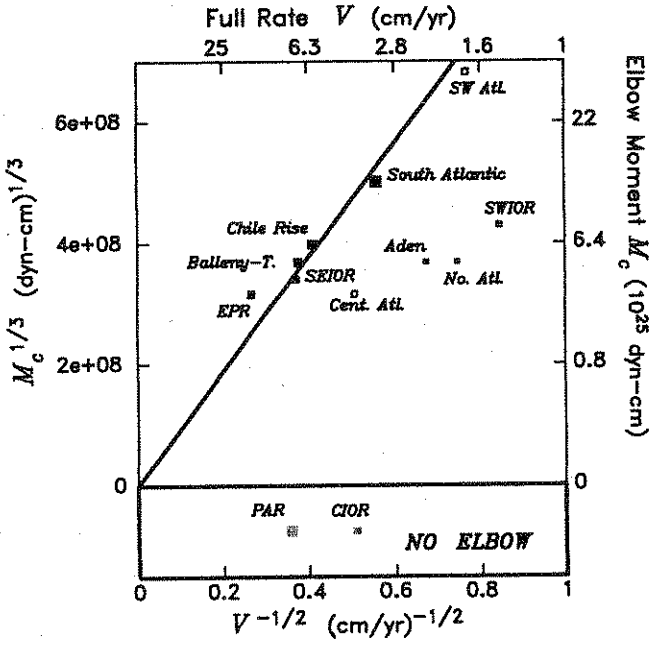

Figure 4. Correlation between spreading rate V and elbow moment, M_c. Axes are linear in $V^{-1/2}$ and $M_c^{1/3}$, both parameters expected to scale like W_{max}. The two regions for which no elbow could be resolved are shown at the appropriate abscissæ in the bottom box. The size of symbols is keyed to the number of samples in each regional dataset. The two regions eliminated from the discussion are shown by open squares. The best regression (constrained to go through the origin of coordinates and weighted by the number of events), is shown as the thick line.

Okal and Romanowicz [1994], we predict a two-segment distribution of earthquakes

$$\log_{10} N = a_1 - \beta_1 \log_{10} M_0 \quad (\beta_1 = 2/3;\ M_0 \le M_c) \quad (3a)$$

$$\log_{10} N = a_2 - \beta_2 \log_{10} M_0 \quad (\beta_2 = 1;\ M_0 \ge M_c) \quad (3b)$$

with the necessary condition of continuity

$$a_2 = a_1 + (\beta_2 - \beta_1) \log_{10} M_c \quad (4)$$

The critical "elbow" moment, M_c, is obtained by noting that it corresponds to a fault width W reaching the lower limit, W_{max} of the seismogenic zone at the center of the offset:

$$M_c = 4\,\mu\,\varepsilon_{max}\,W_{max}^3 = 4\,\mu\,\varepsilon_{max}\,C^3\frac{l^{3/2}}{V^{3/2}} \quad (5)$$

where μ is the rigidity of the medium, ε_{max} the strain release, and $C = 8$ km/Ma$^{1/2}$ $= 0.15$ cm/s$^{1/2}$ a universal constant describing the thickening of the seismogenic lithosphere with age [*Stein*, 1978]. Note that the slope of the regression between $M_c^{1/3}$ and $V^{-1/2}$ on Figure 4 is predicted from (5) to be $(4\mu\varepsilon_{max})^{1/3} \cdot C \cdot l^{1/2}$. Using the above value of C, $\mu = 3 \times 10^{11}$ dyn/cm^2 and $\varepsilon_{max} = 10^{-4}$, this would suggest an average length $l = 52$ km.

In order to determine the constant a_1 in (3*a*), we integrate the total seismic moment release from (3) and equate it to that predicted from plate kinematics. We take into account that TF systems can be deficient in their seismic release, *i.e.*, that not all plate tectonics motion is taken up seismically. We thus define a seismic efficiency parameter, η, characterizing the ratio of seismic moment actually released along the TF system to that predicted by plate kinematic models such as *DeMets et al.*'s [1990]. Previous studies have shown that η ranges from essentially 1 along the Mid-Atlantic Ridge to 0.1 in the Eltanin Region [*Kanamori and Stewart*, 1976; *Stewart and Okal*, 1983; *Okal and Langenhorst*, 2000]. Under this assumption, the total seismic moment released along a TF of length l during a time interval T should be

$$M_\Sigma = \eta\,\mu\,S\,V\,T = \int_0^{+\infty} M_0\,dN \quad (6)$$

The lower bound ($N = 0$) in (6) is, however, limited at a *maximum moment*, M_{max}, obtained when the entire seismogenic area of contact between the two plates, S, ruptures, the seismic slip having the value Δu_{max} reached when the fault width W saturates at W_{max}. Following *Stein* [1978], *Stewart and Okal* [1983] and *Okal and Langenhorst* [2000], we find

$$W_{max} = C\sqrt{\frac{l}{V}};\quad S = \frac{2}{3}\,C\,\frac{l^{3/2}}{V^{1/2}};$$

$$\Delta u_{max} = 2\,l\,C\,\sqrt{l/V}\;\varepsilon_{max} \quad (7)$$

hence

$$M_{max} = \mu S\,\Delta u_{max} = \frac{4}{3}\,\mu\,\varepsilon_{max}\,C^2\,\frac{l^2}{V}. \quad (8)$$

The upper bound ($N \to \infty$) should probably be replaced by a *minimum moment*, M_{min}, since it is doubtful that scaling laws extend to infinitely small events. By substituting (3), (5) and (8) into (6), it is then straightforward to derive

$$a_1 = \log_{10}\left[\frac{\eta\,\mu\,S\,V\,T}{M_c^{1/3}\left[2 + \ln(M_{max}/M_c)\right] - 2M_{min}^{1/3}}\right] \quad (9)$$

and then a_2 using (4). Because M_{min} must be many orders of magnitude smaller than M_c, its exact value has no practical effect on (9).

At this point, we have a complete description of the population of earthquakes along a single TF offset; the next step is to consider a regional spreading system comprised of many offsets of variable lengths l. For each l, we compute populations of moments using (9), which we combine after weighting the results by the number of offsets expected from (2), thus obtaining the full population of moments expected for the entire system. This population can then be analyzed and regressed using a standard algorithm, such as *Okal and Romanowicz'* [1994]. We simply assume that the efficiency η is constant along all TFs in a given region, and thus can take $\eta = 1$ if we are concerned not with the absolute level of seismicity, but only with the shape of the frequency-moment curves.

Unfortunately, this computation cannot be carried out analytically, and a computer simulation is necessary. We use three spreading rates: $V = 2$, 7, and 13 cm/yr, respectively. In practice, it is necessary to introduce a maximum length, l_{max}, which we initially take as 500 km in all three cases. We use $M_{min} = 10^{21}$ dyn-cm, but verified that a smaller value would not affect the results. Figure 5*a* shows the three populations; the curves have been locked at a common value at $M_0 = 10^{24.5}$ dyn-cm to ease

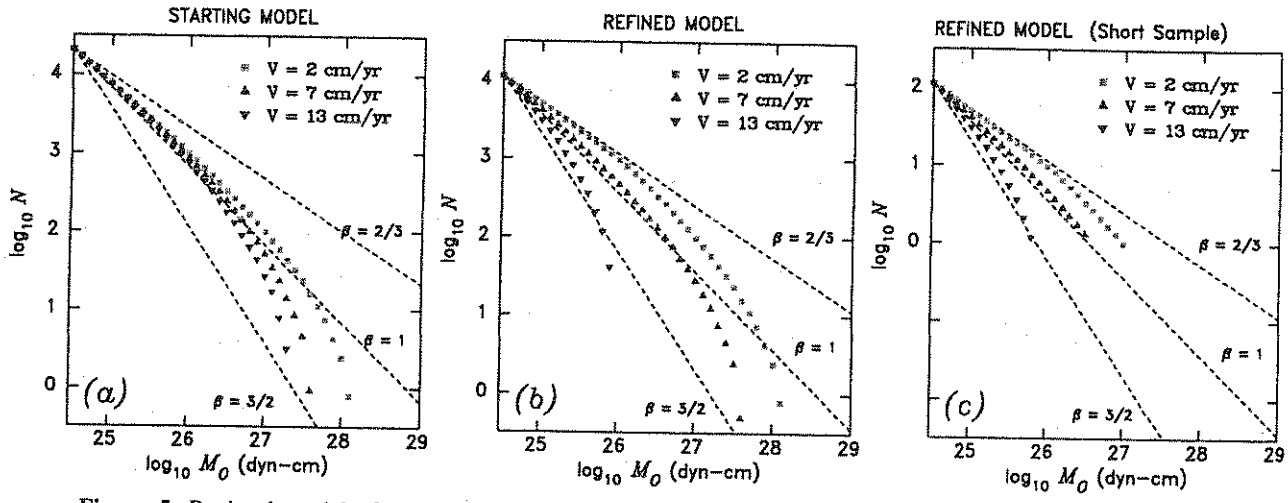

Figure 5. Regional models for populations of strike-slip earthquakes along MOR segments. These models are obtained by combining a population of earthquakes on each TF satisfying (1) and a population of TFs along the MOR segment whose lengths satisfy (2). We apply this model to three segments with different spreading rates. The starting model in *(a)* has a common maximum length l = 500 km. In *(b)*, we reduce the maximum length to 100 km on the fast-spreading segment, and substitute (10) for (2) as a distribution of offsets. In *(c)*, we further consider the effect of a short time-window, which artificially removes the large-moment end of the distributions. See text for details.

comparison; this value is estimated to be the threshold of completeness of the CMT catalogue in remote oceanic areas. It is clear that the populations exhibit curvature, that any regression will lead to inflated values of β, and that higher spreading rates result in generally steeper slopes.

While this model can explain β–values reaching unity, it still predicts a relatively narrow range of variations, with slopes ranging from 0.7 to 1 over the full range of spreading rates. In order to further refine the model, we first note the absence of long offsets on the EPR, and substitute l_{max} = 100 km in the fast-spreading case. Second, we note in *Abbott*'s [1986] study of the slow-spreading Mid-Atlantic Ridge (her Figure 2*a*) that the population seems to saturate at short offset lengths (l < 45 km). This is probably due to the fact that very short offsets are rare on a slow-spreading ridge featuring a broad rift valley. For this reason, we force a two-segment population instead of (2) with an elbow at l_c = 45 km, and a short offset B–value of 0.3:

$$\log_{10} N_l = A_1 - B_1 \log_{10} l \quad (B_1 = 1;\ l \geq l_c) \quad (10a)$$

$$\log_{10} N_l = A_2 - B_2 \log_{10} l \quad (B_2 = 0.3;\ l \leq l_c) \quad (10b)$$

$$A_2 = A_1 + (B_2 - B_1) \cdot \log_{10} l_c \quad (10c)$$

The refined models are shown on Figure 5*b*. They result in a generally greater influence of spreading rate on β–value at low moments, from β ≈ 2/3 at 2 cm/yr, to β ≈ 1.4 at 13 cm/yr. This is essentially what is observed on Figure 1 for the well-sampled part of the dataset, albeit with two exceptions: the SEIOR and SWIOR, both of which have significantly lower-than-modeled values of β.

Finally, we wish to emphasize that our computation is designed to model a fully sampled dataset, *i.e.*, one spanning a time window sufficiently long to allow the detection of an earthquake with moment M_{max}. In the case of the datasets studied on Figure 2, the short life of the CMT project would require moving the vertical scale of Figure 5*b*. For example, a shift of two orders of magnitude in the vertical scale would lead to the diagram on Figure 5*c*, where all points below N = 1 have been eliminated (since it is not possible to count fewer than 1 earthquake). As a result, the slow-spreading ridge will still feature a low-moment regime with β ≈ 2/3, and a resolvable elbow, followed by a range with higher β–value. This fits well the observed population of the South Atlantic Ridge (Figure 2*g*). Along the ridge with intermediate spreading rate, the high-moment population will be suppressed, and no elbow moment will be

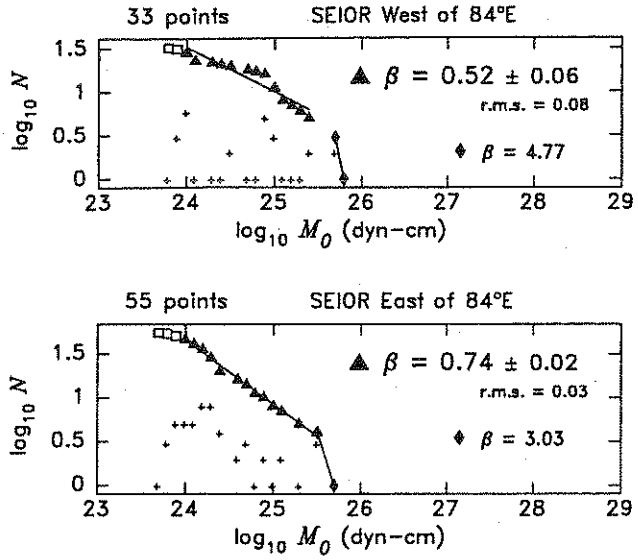

Figure 6. Population statistics for the Southeastern Indian Ocean Ridge (SEIOR) when split into two subsets, West (*Top*) and East (*Bottom*) of 84°E. Note that the western segment is poorly fit, while the eastern one keeps a relatively low β–value, given its fast rate.

resolved, while the entire population will be fit by a single segment with $\beta \approx 1$. This agrees with our observations along the PAR (Figure 2*b*). Finally, the fast-spreading ridge will exhibit both curvature and a very high β–value, approaching 1.5, both features observed along the EPR (Figure 2*a*). We note however that the two large earthquakes in that dataset are not easily explained.

The case of the SEIOR. This region stands out from the rest of our datasets in that it features a regular β–value, ($\beta = 0.73$, close to 2/3), while spreading at a fast rate (7.2 cm/yr). Note also that the fit of the low-moment population is poor, the root-mean-squares residual taking one of its largest values (0.06). We attempted to further partition the region, by excluding its western section, characterized by a large indentation of the plate boundary inside the Antarctic plate, which could express asthenospheric flow between the Kerguelen hotspot and the ridge [*Okal and Stewart,* 1982; *Yale and Phipps Morgan,* 1998]. We use the meridian 84°E as a separator; results would be essentially unchanged if this line were moved a few degrees. As shown on Figure 6, the western dataset is poorly fit by a straight line, but features a trend towards low β; note that it is only marginally above the sampling threshold of 30 events used in this study. On the other hand, the eastern population (55 samples) is much more regular, with a clear elbow at $10^{25.5}$ dyn-cm and a linear distribution of the low-moment population (r.m.s. = 0.03). The β–value is, however, essentially unchanged (0.74), which would suggest that the distribution of offsets along the SEIOR is relatively richer in longer offsets than would be predicted by *Abbott*'s [1986] model. Should many offsets be approximately 50 km in length, this could also explain that the elbow moment of the SEIOR East of 84°E does fit the trend for well-sampled regions (Figure 4). We speculate that the origin of the singular earthquake population along the SEIOR may reside in the "Australian-Antarctic Discordance" documented in this section of the Mid-Oceanic Ridge system [*Weissel and Hayes,* 1971; 1974; *Palmer et al.,* 1993].

The case of the SWIOR. This region is even more puzzling, since it features a β–value less than 2/3, which cannot be predicted by our model. Note that the number of earthquakes (57) in the regional dataset is satisfactory, as is the quality of the fit, as measured by the root-mean-squares residual (0.03). We note that the SWIOR comprises a number of very long TF offsets, separated by very short spreading segments. It is not clear that *Abbott*'s [1986] statistics for populations of TFs would apply along the SWIOR. In addition, the relatively simple models describing the thermal structure of the TF [*McKenzie,* 1967; *Sleep,* 1969; *Sclater et al.,* 1980; *Forsyth and Wilson,* 1980] may be inadequate in the case of a very short ridge segment separating two long TF offsets, and contributing little heat to the system. This is precisely the geometry of the Andrew Bain TF, the site of the event of 10 November 1942, at 1.3×10^{28} dyn-cm the largest ever recorded on an oceanic TF [*Okal and Stein,* 1942] (this historical event not being part of our dataset). The conclusion of that study was that, in contrast to the case of most other oceanic TFs [*Engeln et al.,* 1986], one could not accommodate the size of the 1942 earthquake on the Andrew Bain TF using universal scaling laws and thermal models. This departure from universal models may explain the low β–value obtained in this region.

Further study of the seismicity and ridge morphology of both the SEIOR and SWIOR is clearly warranted but falls beyond the scope of the present paper.

Finally, we wish to comment briefly on *Bird et al.*'s [2002] concurrent paper in this volume, which comes to a strikingly different conclusion, namely that they find no dependence of β on V. The most likely explanation to this difference is that we use *Rundle*'s [1989] simpler statistics, as opposed to *Kagan*'s [1993], which Bird *et al.* utilize. Since we can explain most of our observations (with the exception of the South Indian ridges) with the simpler model, we see no reason to use the more complex one. Furthermore, we note that Bird *et al.* separate the worldwide dataset into only three subsets of equal popula-

tion, ranked by spreading rate V, but irrespective of geographical area. This algorithm would be acceptable if the whole earthquake population was evenly distributed with V; however, it is bound to create biases when the slowest ridges (SWIOR) are significantly undersampled (only 57 events), and the strongest contributor (South Atlantic; 199 events) features the expected β–value.

5. CONCLUSION

In regional datasets of strike-slip earthquakes occurring on transform faults of the Mid-Oceanic Ridge system, we have established the existence of a correlation between the spreading rate V and the β–value characterizing the lower-moment end of the earthquake population. While five regions can be fit with the predicted $\beta = 2/3$, fast spreading ridges such as the EPR and the PAR have significantly greater values of β. This property can be explained by a simple model combining a power law distribution of earthquakes on a single transform, with a second power law distribution of the lengths of transforms along a given ridge segment. Using this model, we can readily explain the apparent higher β–values featured by transforms on fast spreading ridges without invoking an intrinsic change of scaling laws, and hence of physical properties, on the relevant ridge segments. There remain the cases of the two Southern Indian Ocean Ridge systems, the SWIOR where a strong deficiency of ridge segment may profoundly alter the thermal regime of the faults, and the SEIOR, where the presence of the Australian-Antarctic Discordance may invalidate the distribution of transform lengths proposed by *Abbott* [1986].

Acknowledgments. This research was finalized while ARL was the recipient of a grant from the Deutscher Akademischer Austauschdienst at Universität Potsdam. Seth Stein pointed out the study by Dallas Abbott, who also gave us valuable insight in her work. We acknowledge helpful reviews by Cliff Frohlich and Barbara Romanowicz. EAO thanks the people of Rapa Nui for hospitality in ultimate isolation, propitious to scientific writing.

REFERENCES

Abbott, D.H., A statistical correlation between ridge crest offsets and spreading rate, *Geophys. Res. Letts., 13,* 157–160, 1986.

Bird, G.P., Y.Y. Kagan, and D.D. Jackson, Plate tectonics and earthquake potential of spreading ridges and oceanic transform faults, *Amer. Geophys. Un. Geophys. Monog.,* this volume, 2002.

DeMets, D.C., R.G. Gordon, D.F. Argus, and S. Stein, Current plate motions, *Geophys. J., 101,* 425–478, 1990.

Dziewonski, A.M., A. Friedman, D. Giardini, and J.H. Woodhouse, Global seismicity of 1982: Centroid moment tensor solutions for 308 earthquakes, *Phys. Earth Planet. Inter., 33,* 76-90, 1983.

Engeln, J.F., Seismological studies of the tectonics of divergent plate boundaries, *Ph.D. Dissertation,* 138 pp., Northwestern Univ., Evanston, Illinois, 1985.

Engeln, J.F., D.A. Wiens, and S. Stein, Mechanisms and depths of Atlantic transform fault earthquakes, *J. Geophys. Res., 91,* 548–578, 1986.

Forsyth, D.W., and B. Wilson, Three-dimensional temperature structure of a ridge-transform-ridge system, *Earth Planet. Sci. Letts., 70,* 355–362, 1984.

Frohlich, C.F., and S.D. Davis, Teleseismic *b*-values: or, much ado about 1.0, *J. Geophys. Res., 98,* 631–644, 1993.

Gutenberg, B., and C.F. Richter, Earthquake magnitude, intensity, energy and acceleration, *Bull. Seismol. Soc. Amer., 32,* 163–191, 1942.

Kagan, Y.Y., Statistics of characteristic earthquakes, *Bull. Seismol. Soc. Amer., 83,* 7–24, 1993.

Kagan, Y.Y., Seismic moment–frequency relation for shallow earthquakes: Regional comparison, *J. Geophys. Res., 102,* 28735–2852, 1997.

Kagan, Y.Y., Universality of the seismic moment-frequency relation, *Pure Appl. Geophys., 155,* 537–573, 1999.

Kanamori, H., and G.S. Stewart, Mode of the strain release along the Gibbs Fracture Zone, Mid-Atlantic Ridge, *Phys. Earth Planet. Inter., 11,* 312–332, 1976.

McKenzie, D.P., Some remarks on heat flow and gravity anomalies, *J. Geophys. Res., 72,* 6261–6273, 1967.

Molnar, P., Earthquake recurrence intervals and plate tectonics, *Bull. Seismol. Soc. Amer., 69,* 115–133, 1979.

Okal, E.A., and A.R. Langenhorst, Seismic properties of the Eltanin Transform System, South Pacific, *Phys. Earth Planet. Inter., 119,* 185–208, 2000.

Okal, E.A., and B.A. Romanowicz, On the variation of *b*-value with earthquake size, *Phys. Earth Planet. Inter., 87,* 55-76, 1994.

Okal, E.A., and S. Stein, The 1942 Southwest Indian Ocean Ridge Earthquake: Largest ever recorded on an oceanic transform, *Geophys. Res. Letts., 14,* 147-150, 1987.

Okal, E.A., and L.M. Stewart, Slow earthquakes along oceanic fracture zones: evidence for asthenospheric flow away from hotspots?, *Earth Plan. Sci. Lett., 57,* 75-87, 1982.

Palmer, J., J.-C. Sempéré, D.M. Christie, and J. Phipps Morgan, Morphology and tectonics of the Australian-Antarctic discordance between 123°E and 128°E, *Mar. Geophys. Res., 15,* 121–152, 1993.

Press, W.H., B.P. Flannery, S.A. Teukolsky, and W.T. Vetterling, *Numerical Recipes*, Cambridge Univ. Press, 818 pp., 1986.

Romanowicz, B.A., and J.B. Rundle, Scaling relations for large earthquakes, *Bull. Seismol. Soc. Amer., 83,* 1294–1297, 1993.

Rundle, J.B., Derivation of the complete Gutenberg-Richter magnitude-frequency relation using the principle of scale invariance, *J. Geophys. Res., 94,* 12337–12342, 1989.

Sclater, J.G., C. Jaupart, and D. Galson, The heat flow through oceanic and continental crust and the heat loss of the Earth, *Revs. Geophys. Space Phys., 18,* 269–311, 1980.

Sleep, N.H., Sensitivity of heat flow and gravity to the mechanism of sea-floor spreading, *J. Geophys. Res., 74,* 542–549, 1969.

Stein, S., A model for the relation between spreading rate and oblique spreading, *Earth Planet. Sci. Letts., 39,* 313–318, 1978

Stewart, L.M., and E.A. Okal, Seismicity and aseismic slip along the Eltanin Fracture Zone, *J. Geophys. Res., 88,* 10495-10507, 1983.

Weissel, J.K., and D. Hayes, Asymmetric sea-floor spreading South of Australia, *Nature, 231,* 518–522, 1971.

Weissel, J.K., and D. Hayes, The Australian–Antarctic discordance: new results and implications, *J. Geophys. Res., 79,* 2579–2587, 1974.

Yale, M.M., and J. Phipps Morgan, Asthenosphere flow model of hotspot-ridge interactions: a comparison of Iceland and Kerguelen, *Earth Planet. Sci. Letts., 161,* 45–56, 1998.

A.R. Langenhorst, Geophysical Fluid Dynamics Laboratory, Forrestal Campus, Route 1, Princeton, NJ 08542; amy@earth.nwu.edu.

E.A. Okal, Department of Geological Sciences, Northwestern University, Evanston, IL 60208.; emile@earth.nwu.edu.